Strategies for active tuning of Wave Energy Converter hydraulic power take-off mechanisms

C.J. Cargo, A.J. Hillis*, A.R. Plummer

Department of Mechanical Engineering, University of Bath, Bath BA27AY

Abstract

This paper presents a study of practically implementable active tuning methods for a Wave Energy Converter (WEC) power take-off (PTO). It is distinguished from other simulation studies by the level of detail and realism in the inputs and the PTO model. Wave data recorded at the European Marine Energy Centre is used to derive input data for a detailed component level model of a hydraulic PTO. A methodology is presented for obtaining the optimum PTO damping co-efficient for a given sea state, and an open loop active tuning method is used to adjust the PTO parameters to achieve this optimum damping in service. The investigation shows that tuning of a hydraulic PTO to an estimated wave frequency is a difficult task due to sea state estimation errors and the complex dynamics of a realistic PTO. Preview knowledge of the future waves was shown to provide no meaningful improvement in energy capture for the device under investigation. Significantly, power gains observed in similar work using simplified linear PTO models or simplified sea states are not seen here, demonstrating that over-simplification of the PTO during the simulation phase of WEC development could lead to incorrect design decisions and subsequent additional delay and cost.

Key words: wave energy, hydraulic PTO, power optimization, irregular waves

*Corresponding author

Email address: a.j.hillis@bath.ac.uk (A.J. Hillis)

1. Introduction

The optimization of wave energy converter (WEC) hydraulic power take-offs (PTO) in sea states of varying wave amplitude, direction, and frequency is a significant problem. Sub-optimal configuration can result in very inefficient energy conversion [1], so understanding the design trade-offs is key to the success of the technology. This work focuses on a generic point absorber type WEC. Previous work by the authors has considered the optimisation of this device for regular waves [2] and synthesised irregular waves [3] to gain an understanding of the fundamental issues. This paper considers real wave data from the European Marine Energy Centre (EMEC) based in Orkney, Scotland. It presents techniques to analyse the wave energy resource at a particular site by using statistics that are calculated from the raw data. A method to calculate the wave excitation force from the raw wave displacement is presented and this is then used as the input to a simulation model. This provides a prediction of how the WEC will behave and the power which can be generated in real wave conditions.

PTO tuning is investigated using the real data and compared to the results found previously [2, 3]. Real time tuning methods are analysed to determine the best method to maximise power generation by updating the PTO damping. Active and passive methods are examined which tune the PTO to a wave frequency calculated from different horizons of wave data.

2. Background

Previous work has focused on developing control methods for point absorbers to maximize the energy absorbed. Falcao [4] used a simplified hydraulic PTO unit connected to a point absorber to develop an algorithm to optimize the converter. The algorithm was shown to be weakly dependent on wave period and independent of wave height when simulated in real sea conditions and to produce power levels similar to a fully linear PTO unit. This work was continued in Falcao [5] to include a strategy for phase control by latching to increase the absorbed power further. In Babarit et al. [6] three different latching control strategies are compared to show their effectiveness in different sea states with all three strategies giving a

considerably increased efficiency in irregular waves. In Yavuz et al. [7] work focuses on assessing the performance of a tuneable point absorber by trying to fulfil the condition of resonance by varying the PTO characteristics. Results showed a maximum power capture of 50 per cent of the rated power in regular waves. This work was continued in Yavuz et al. [8] with irregular waves to show that power capture can be maximized by continuously tuning the natural frequency of the device to the incoming wave frequency. More recently, in Folley and Whittaker [9], a new control method called active bipolar damping or declutching is proposed which tries to shift the buoy's velocity so it is in phase with the wave force. When compared theoretically to other methods, it shows a higher power capture than optimum linear damping without the requirement of reactive energy storage. This control method has been investigated in Babarit et al. [10] using a hydraulic PTO and compared to a control method which tries to mimic the continuous behaviour of a viscous damper. Results show greater power levels from the declutching control method with the added advantage of requiring a less complex system. Most of these investigations use linearized models and do not consider real hydraulic circuits and components in their investigations.

3. Hydrodynamics of the WEC

A point absorber type device is used for this study and is the same as that used in [2] and [3]. A diagram of the heaving buoy is shown in Fig. 1, and it has a mass of 39 tonnes, a radius of 2m and a draft of 4m. A point mass acting at the centre of the buoy is assumed. The governing equation of motion for the buoy in heave is

$$m\ddot{x} = f_h(t) + \Phi(t) \tag{1}$$

where m is the mass of the buoy, $\ddot{x}$ is the buoy's acceleration, $f_h(t)$ is the total wave force and $\Phi(t)$ is the mechanical force created by the PTO and moorings. Assuming linear wave theory, the wave force can be approximated as

$$f_h(t) = f_e(t) + f_r(t) + f_{hs}(t) \tag{2}$$

where $f_e(t)$ is the excitation force produced by an incident wave on an otherwise fixed body, $f_r(t)$ is the radiation force and $f_{hs}(t)$ is the hydrostatic buoyancy force. For a regular wave of frquency ω the excitation force is given by

$$f_e(t) = Re(F_e e^{j\omega t}) \tag{3}$$

where F_e is the complex excitation force amplitude. Following the approach described in [3] and using the assumptions of [11] and Hulme [12], for a hemispherical body that is small in comparison to the incident wavelength, F_e may be approximated by

$$F_e \approx \frac{H\rho}{\omega}\sqrt{\frac{\pi}{3}g^3 r^3 \epsilon e^{-2kl}} \tag{4}$$

where H is the free surface elevation, ρ is the water density, g is the acceleration due to gravity, r and l are the radius and half-height of the buoy, ϵ is Havelock's dimensionless damping coefficient computed by Hulme [12] and k is the wave number ($k = \frac{\omega^2}{g}$) given by the deep water dispersion equation.

The radiation force $f_r(t)$ can be decomposed into components in phase with the buoy's acceleration and velocity [11] [13] so that

$$f_r(t) = -A(\omega)\ddot{x} - B(\omega)\dot{x} \tag{5}$$

where $A(\omega)$ is the added mass coefficient and $B(\omega)$ is the radiation damping coefficient, which may be approximated in this case to [11] [12]

$$B(\omega) \approx \omega\rho\left(\frac{2\pi}{3}\right) r^3 \epsilon e^{-2kl} \tag{6}$$

For small heave displacements, the hydrostatic force $f_{hs}(t)$ can be linearised so that

$$f_{hs}(t) = -\rho g \pi r^2 x \tag{7}$$

4. Hydraulic PTO mechanism

The aim of the PTO is to convert the irregular wave input into a smooth electrical power output by decoupling the power capture and power generation

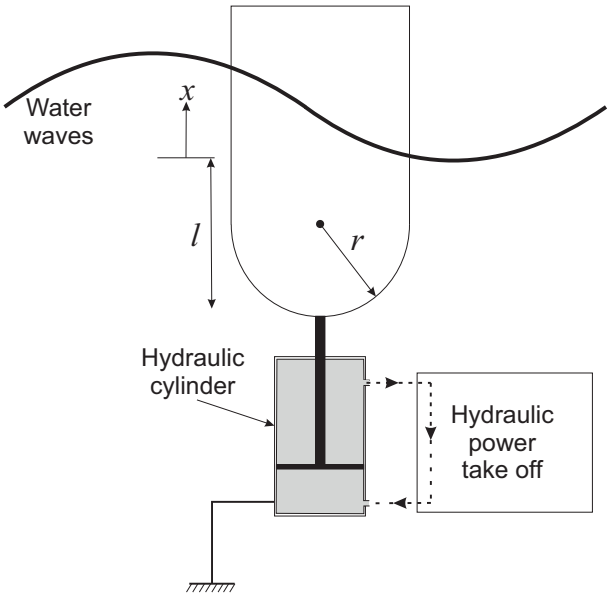

Figure 1: Schematic diagram of the WEC

processes. Hydraulic PTOs are generally used in WECs due to their advantages for dealing with low frequency, high force wave inputs and their high power density and robustness.

The hydraulic PTO used in this simulation model is shown in Figure 2. The simplified circuit excludes components such as filters and coolers which would be required in the real hydraulic system. The heave motion of the buoy drives a double-acting equal area hydraulic piston within a fixed cylinder to pump hydraulic oil through rectification circuit to provide unidirection flow through a hydraulic motor. The pressure difference between the high and low pressure accumulators drives a variable displacement hydraulic motor, which drives an electrical generator. The accumulators are intended to smooth the pressure differential across the hydraulic motor and therefore achieve synchronous power generation. The thermodynamic transformations in the accumulators are assumed to be isentropic, which is a reasonable assumption considering the cycle time of the device. The generator is modelled as a simple rotational damper with variable damping coefficient allowing its resistive torque to be altered. In a real circuit, there will be external leakage from the motor to tank. Therefore, to replenish the circuit and avoid cavitation in the cylinder, an additional accumulator is used to maintain a minimum system pressure of 10 bar. Pressure relief valves are used to limit the

peak system pressure to 350 bar and protect hydraulic components.

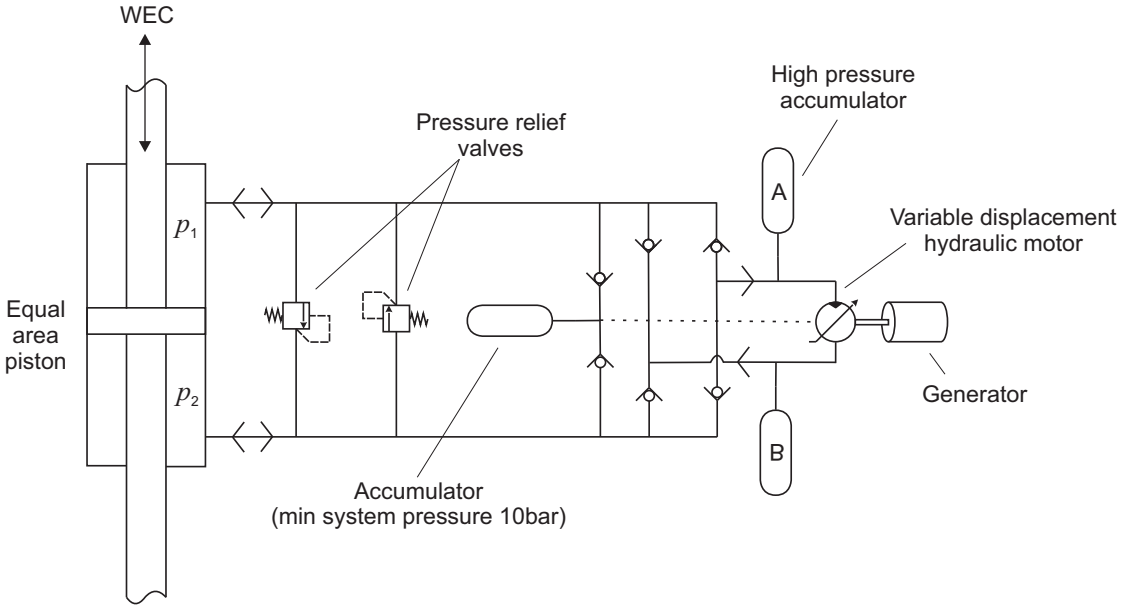

Figure 2: Hydraulic PTO circuit diagram

In reality there will be losses throughout the hydraulic circuit including friction in the piston and pipework, leakage in the motor and torque losses due to friction in the motor and generator. These losses will be system specific and are approximated here based on experience.

The PTO force is given by

$$\Phi = (p_1 - p_2)A_p - f_{fr} \tag{8}$$

where p_1 and p_2 are the pressures in the piston chambers, A_p is the piston area and f_{fr} is the cylinder friction force, given by

$$f_{fr} = f_c sign(\dot{x}) + f_v \dot{x} \tag{9}$$

where f_c and and f_v are the Coulomb and viscous friction coefficients, respectively. The details for calculating cylinder pressures are provided in [3].

The mechanical power captured by the PTO is given by

$$P_{cap} = \Phi \dot{x} \tag{10}$$

The power generated by the PTO is not equal to the captured power P_{cap} due to system losses in the hydraulic circuit and electrical generator. The generated power may be caluclated from

$$P_{gen} = T_m \omega_m \tag{11}$$

where T_m and ω_m are the motor torque and angular velocity, respectively. The motor torque is calculated from[14]

$$T_m = x_m D_m (p_A - p_B) - C_f D_m (p_A - p_B) - C_v D_m \mu \omega_m \tag{12}$$

where x_m is the fraction of maximum displacement D_m of the hydraulic motor displacement, μ is the dynamic viscosity of the oil and p_A and p_B are the accumulator pressures. Again, the details for calculating accumulator pressures are provided in [3]. C_v and C_f are dimensionless viscous friction and Coulomb friction co-efficients representing motor losses according to the Wilson model [14]. Slip losses are also included, and are calculated as[14]

$$q_m - \frac{C_s D_m (p_A - p_B)}{\mu} = x_m D_m \omega_m \tag{13}$$

where q_m is the flowrate to the motor and C_s is the dimensionless slip coefficient. The motor angular velocity can be calculated from rotational acceleration, which is given by

$$\dot{\omega}_m = \frac{T_m - T_g}{J} \tag{14}$$

where T_g and J are the torque and inertia of the generator.
Assuming no losses, the generator torque is given by

$$T_g = C_g \omega_m \tag{15}$$

where C_g is the damping coefficient of the generator.
Table 1 shows the component parameters in the PTO. These values are not based on any specific design but are a representation of suitable sizing for the buoy size. In this idealised case the effect of the boost pump is negligible and the

electrical generator is assumed to be 100% efficient so the electrical power generated can be equated to the mechanical power generated by the PTO. The high pressure accumulator ('A') has a relatively low pre-charge pressure to ensure that it charges even in calm wave conditions.

Maximum system pressure	350 bar
Equal area piston	
Area	$0.007\,\mathrm{m}^2$
Stroke Limit	$\pm 2.5\,\mathrm{m}$
HP Gas accumulator 'A'	
Pre-charge Pressure	30 bar
Volume	200 L
γ	1.4
LP Gas accumulator 'B'	
Pre-charge Pressure	10 bar
Volume	200 L
γ	1.4
Variable Displacement Motor	
Capacity	180 cc/rev
Generator	
Damping coefficient	$2.5\,\mathrm{Nm/(rad/s)}$
Inertia	$2\,\mathrm{kgm}^2$
Oil Properties	
Viscosity	50 cSt
Density	$850\,\mathrm{kg/m}^3$

Table 1: PTO component values

Table 2 shows the parameters of all the other components required to calculate the losses.

Cylinder	
Coulomb friction (f_c)	3500 N
Viscous friction coefficient (f_v)	$100\,\mathrm{N/(m/s)}$
Variable Displacement Motor	
C_f	0.014
Check Valve	
Valve constant (K_v)	$8.5\times\ 10^{-6}$
Cracking Pressure	0.3 bar
Pipework	
Diameter (d)	50 mm
Total Length (l)	10 m

Table 2: PTO unit component loss parameters

5. Wave Data Analysis

Real ocean waves are random but there are key parameters which can be calculated from recorded wave elevation data to analyse and compare different sea states. These parameters are calculated from the frequency moments of the variance spectrum (m_a) [15]. The frequency spectrum (S_n) is given by the Fast Fourier Transform (FFT) of the wave elevation. Figure 3 shows the spectrum as a result of taking the FFT of a 30 minute duration data packet sampled at 1.28Hz. The raw FFT produces a noisy spectrum which could produce erroneous results when used to calculate key parameters of the underlying sea state. A smoothed spectrum may be obtained by passing the raw amplitude spectrum through a polynomial filter. In this case a Savitzky-Golay filter was used [16], though this is arbitrary. A third order polynomial filter was used with a frame size of 81. In subsequent analyses, both raw and smoothed spectra are used for PTO tuning and the results are compared.

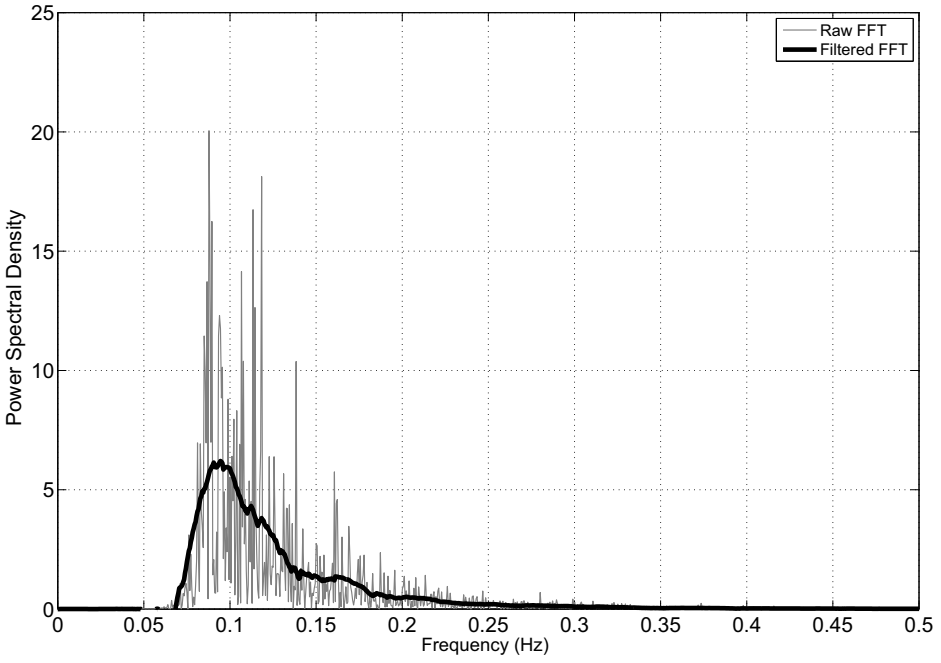

Figure 3: Example frequency spectrum of measured wave data

The moments of the variance spectrum (m_a) for a=-1,0,1,2, are calculated from

[15]:

$$m_a = \sum_{i=1}^{N} S_{n_i} \omega_i^a \Delta\omega = \int_0^{\omega_N} S_n \omega^a d\omega \tag{16}$$

where N is chosen so as to include the frequency range (ω_i to ω_N) containing significant power (e.g. 0-0.25Hz in Figure 3.)

The significant wave height (H_s), peak period (T_p), energy period (T_e) and wave power flux (P_{flux}) are key parameters[15]. The significant wave height is the average of the wave heights of the third largest waves and the peak period is the wave period corresponding to the most energetic waves in the spectrum and is given by

$$H_s = 4\sqrt{m_0} \tag{17}$$

The peak period T_p is given by

$$T_p = \frac{1}{f_p} \tag{18}$$

where f_p is the frequency in Hz corresponding to maximum S_n.

The energy period (T_e) is given by

$$T_e = \frac{m_{-1}}{m_0} \tag{19}$$

The total wave power flux (P_{flux}) of the spectrum is the scalar sum over the frequency range, and is found from

$$P_{flux} = \frac{1}{2a} \sum_{i=1}^{N} P_{wave_i} \tag{20}$$

Artificial irregular wave elevation and excitation force profiles can be created using the random-phase method [5] though this results in periodic signals which are not realistic. Alternatively, they can be generated by shaped filtering of white noise [17, 18] which is more realistic. Real waves are non repeating and their frequency spectrum may have more than one significant peak. This work uses real wave data collected from test sites to determine if the trends and methods which have been found previously [2] are applicable to real waves.

EMEC has a number of data collection buoys in different locations around their

site in Orkney. Data for the months of April and October 2011 were obtained for one of the locations (Billia Croo Buoy E). The data is for the wave heave displacement and it is split into 30 minute packets with a sampling frequency of 1.28 Hz.

The wave parameters defined in equations 17 to 20 were calculated for each individual data packet and the results for both months are compared in Figures 4 to 7. They reveal that the average power available in April was lower than October. October had more occurrences of the lowest level of wave power (<30 kW/m) but there were also more large wave powers (>100 kW/m), which indicates more variable weather (Figure 7). The average values of terms relating to wave period are lower for October but the variance is lower in April. In particular, there are more short period waves in October (Figure 5). This may indicate a changing of the dominant wave frequency through the year in this location.

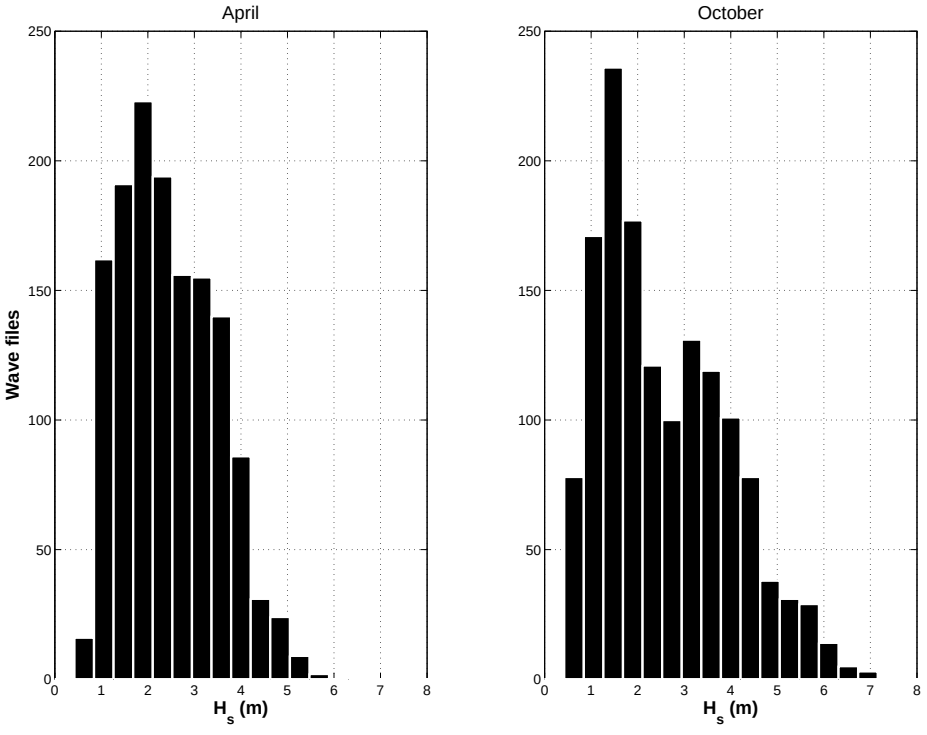

Figure 4: Frequency histogram showing the significant wave height in April and October

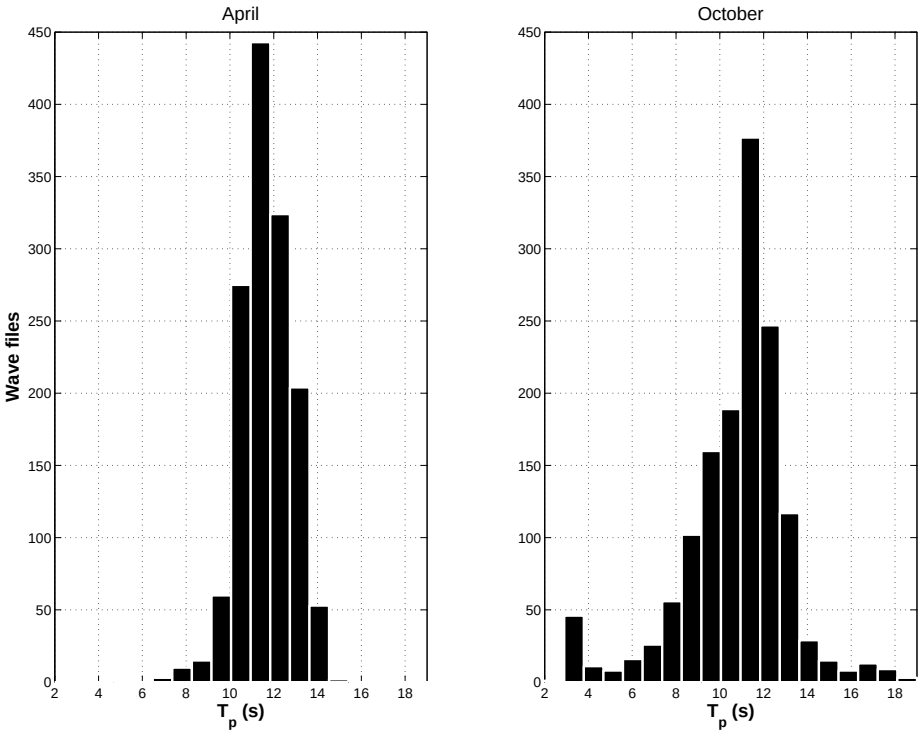

Figure 5: Frequency histogram showing the peak period in April and October (from filtered spectrum)

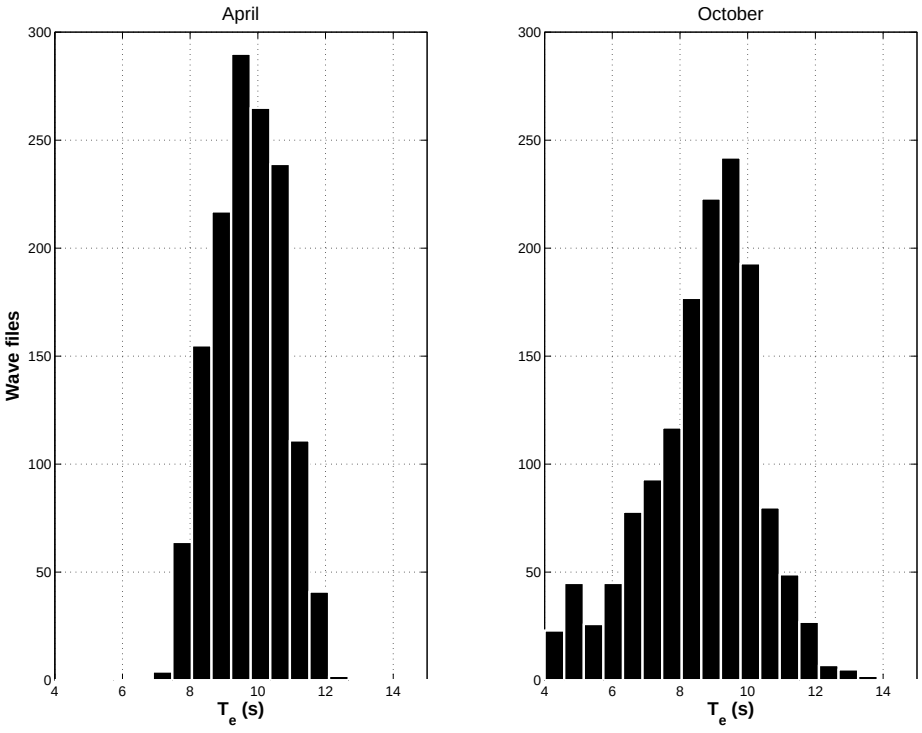

Figure 6: Frequency histogram showing the energy period in April and October

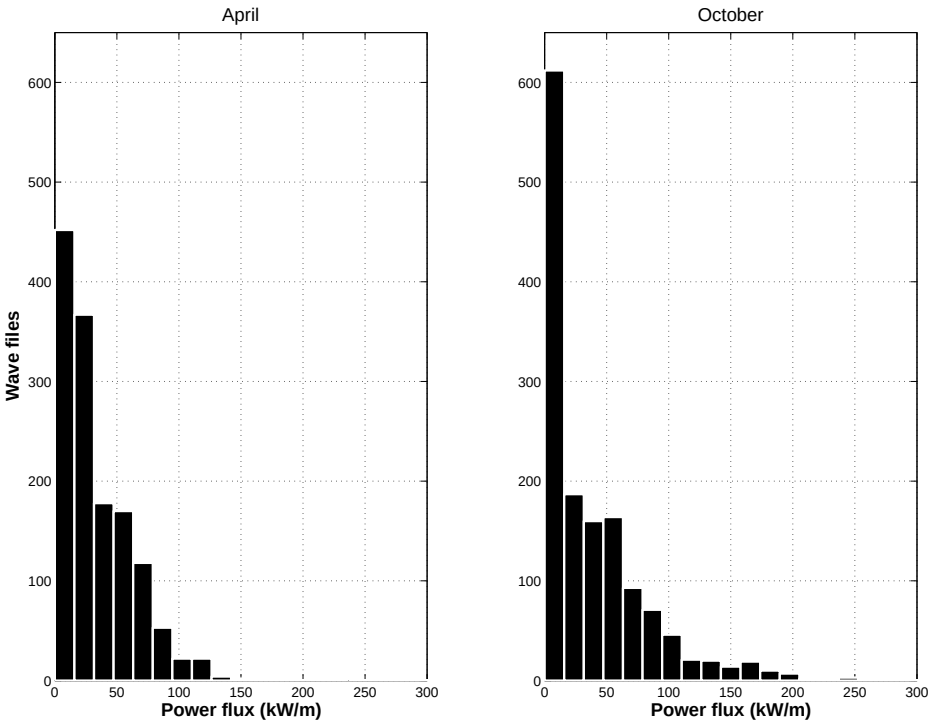

Figure 7: Frequency histogram showing the wave power flux in April and October

6. Generating a Wave Excitation Force Signal from wave elevation data

The simulation model uses wave excitation force as the input to the hydrodynamic model so it is necessary to create a wave excitation force signal from the wave elevation data. The FFT of the wave displacement gives the discrete frequency components (ω_i) and their corresponding amplitude (X_{w_i}) and phase (ϕ_i). Assuming a finite number of wave components, the wave excitation force coefficient $\Gamma(\omega_i)$ of each wave component can be calculated as follows. Equations 4 and 6 can be combined to obtain an expression for the wave excitation force amplitude F_e as a function of the radiation damping coefficient $B(\omega)$:

$$F_e \approx H\sqrt{\frac{B(\omega)g^3\rho}{2\omega^3}} \tag{21}$$

According to Falnes [11], Fe can be expressed in terms of the wave excitation force coefficient $\Gamma(\omega)$ as:

$$F_e = \Gamma(\omega)\frac{H}{2} \tag{22}$$

Comparing equation 21 with equation 22, it can be seen that

$$\Gamma(\omega_i) = \frac{2}{H}F_e \approx \sqrt{\left(\frac{2g^3\rho B(\omega_i)}{\omega_i^3}\right)} \tag{23}$$

The excitation force can then be calculated from

$$f_e(t) = \sum_{i=1}^{n} \Gamma(\omega_i) X_w(\omega_i) \cos(\omega_i t + \varphi_i) \tag{24}$$

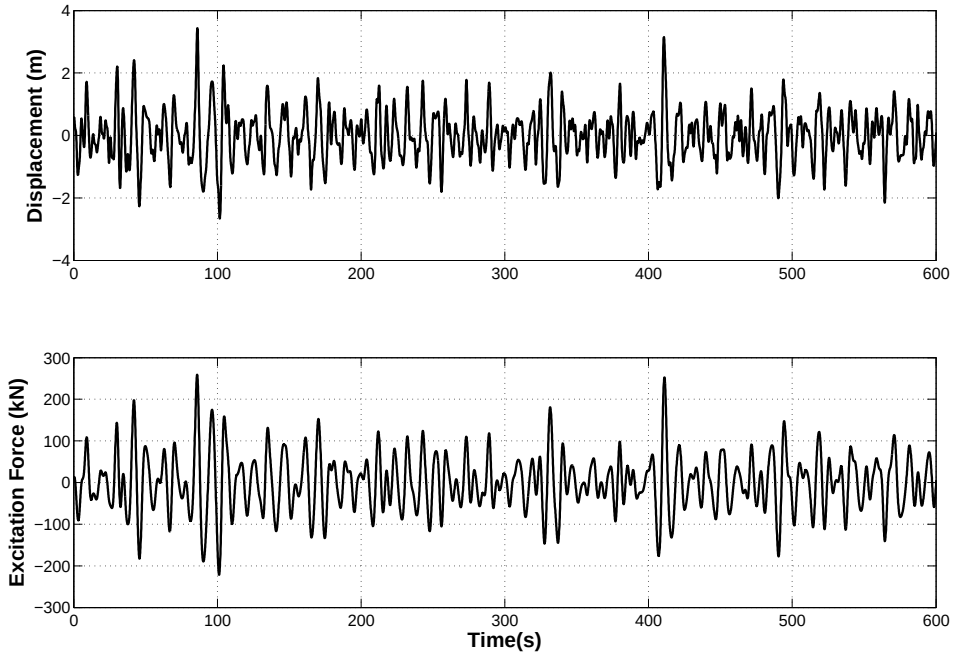

Figure 8: Wave displacement and excitation force for an example EMEC file

Figure 8 shows a 600 s section of an example EMEC file with the wave displacement and the calculated wave excitation force. In the time domain, Figure 9 shows that the WEC behaves in a similar manner to that in irregular waves produced by the random phase method [2], with induced body stall and Coulomb type PTO force evident.

Since the wave profile is non-repeating the energy stored in the accumulators will not achieve a pseudo-steady state over a fixed time period as seen with a

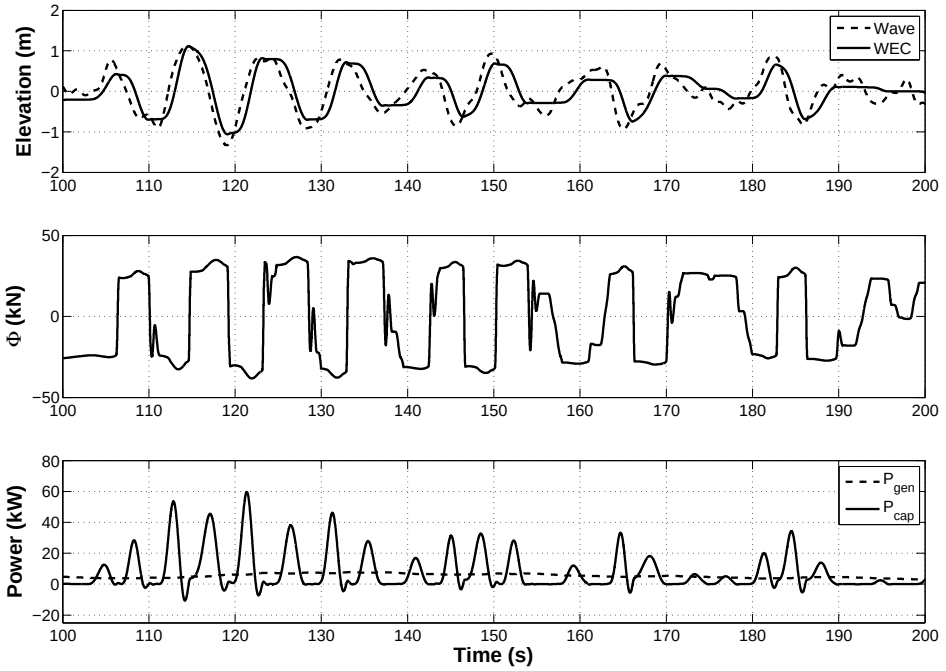

Figure 9: WEC and PTO behaviour in the example EMEC file

repeating wave force input [3]. Therefore, to negate the effect of the added energy stored in the accumulators giving an inaccurate result for the generated power (P_{gen}) and PTO efficiency (η_{pto}) the model is analysed over the largest possible time period.

7. PTO Tuning in Real Seas

Previous work [3] demonstrated a relationship between the peak wave period (T_p) and the optimum PTO damping (α_{opt}) for waves created using the Pierson-Moskowitz spectrum and the random phase method:

$$\alpha_{opt}(T_p) = C_g \left(\frac{x_m D_m}{A_p} \right)^2 \tag{25}$$

where A_p represents the piston area, C_g is the generator damping coefficient, D_m is the hydraulic motor capacity and x_m is the fraction of maximum motor displacement. Here, the piston area is fixed and the PTO damping is optimised for a given T_p by varying the motor capacity and generator load.

It is important to determine if this, or any other relationship, exists for real wave

data. Therefore, a number of wave packets were chosen in both months with $H_s \approx 2.5\,\text{m}$ and T_p ranging from 8 - 14 s approximately. For each of the wave packets an optimisation algorithm was used to maximise P_{gen} and give α_{opt} to determine any trends between it and the wave parameters.

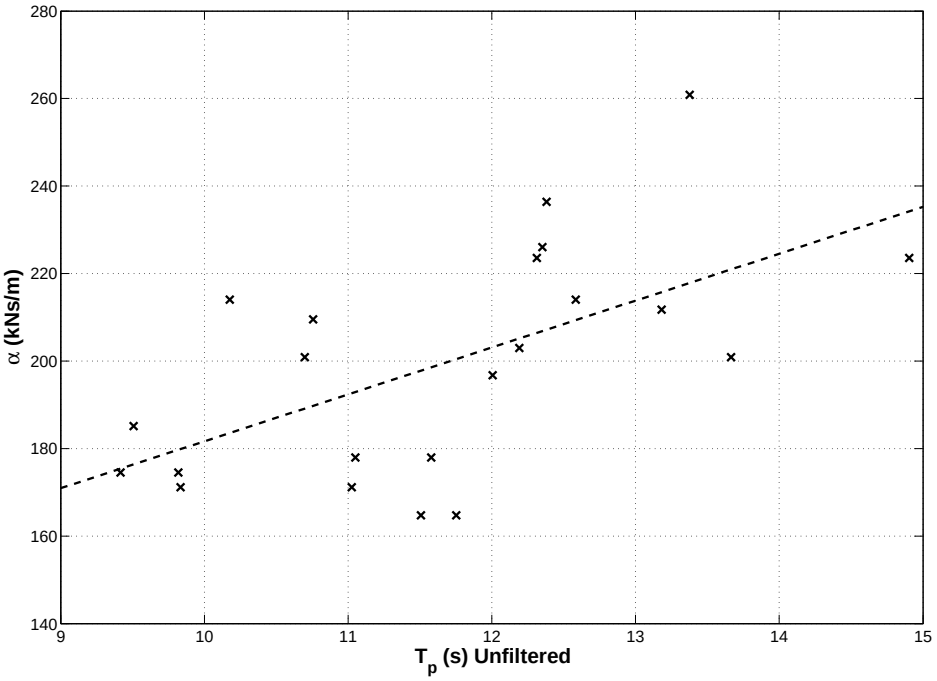

Figure 10: Optimum PTO damping vs peak wave period with filtered spectrum

Wave Parameter	Hydraulic PTO
T_p (Filtered)	74.9
T_p (Unfiltered)	95.3
T_e	56.1

Table 3: Norm of the residuals for the fit between the optimum PTO damping and the different wave parameters

Figures 10, 11 and 12 show that the correlation between T_p and α_{opt} is better when T_p is calculated from the filtered spectrum. However, Table 3 shows that the norm of the residuals, an indicator of the goodness of the correlation, is lowest for the fit between the energy period (T_e) and α_{opt}.

When comparing all the trend lines, it is clear from Figure 13 that the filtered T_p and unfiltered T_p trends are very similar. It also shows that the trend for T_e and T_p using a Pierson-Moskowitz spectrum are similar. In terms of power, Figure 14

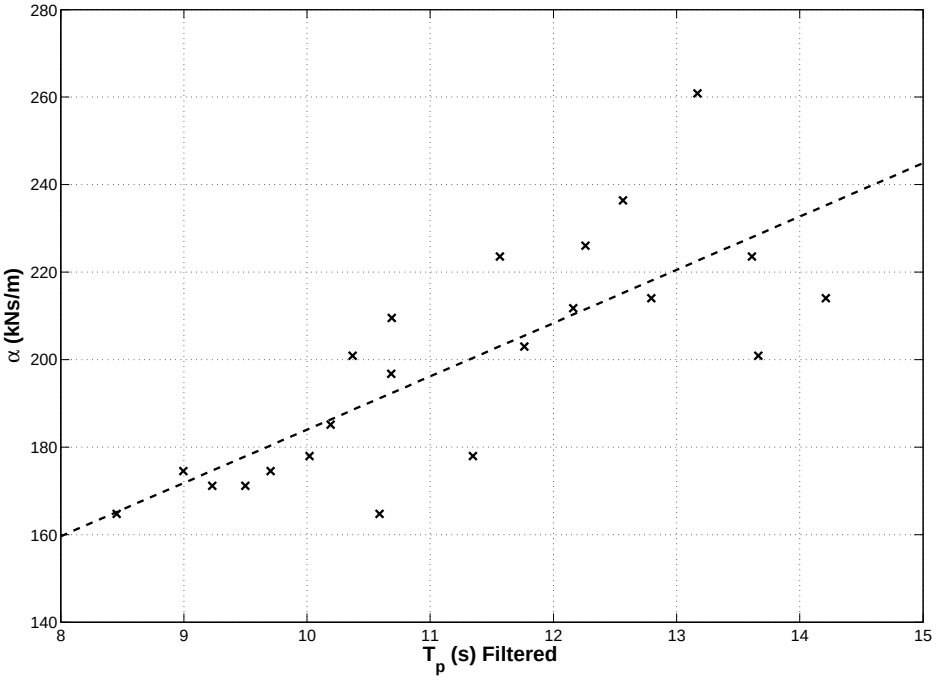

Figure 11: Optimum PTO damping vs peak wave period with unfiltered spectrum

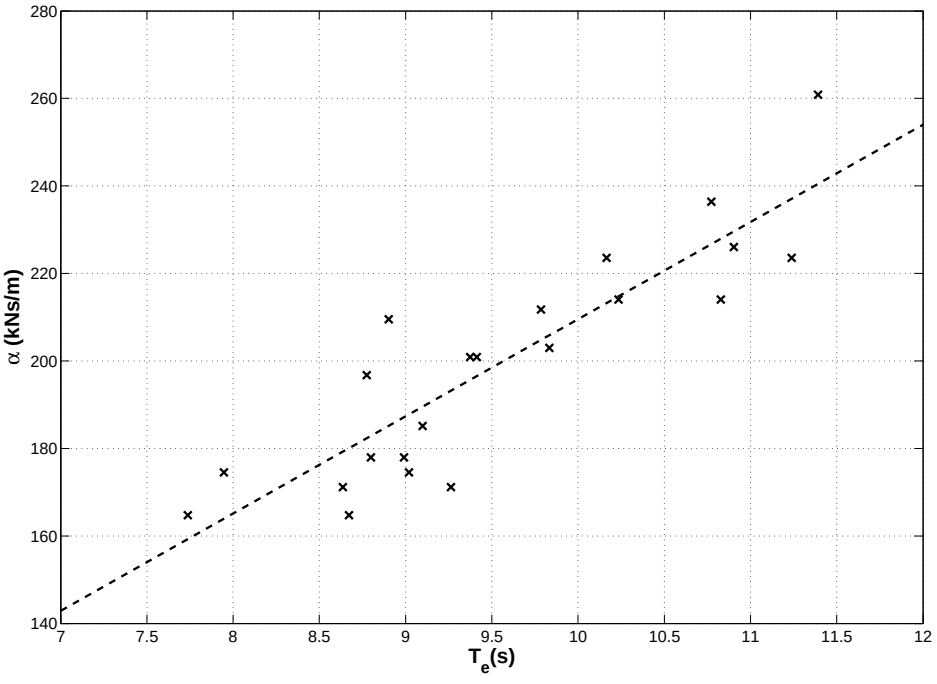

Figure 12: Optimum PTO damping vs energy period

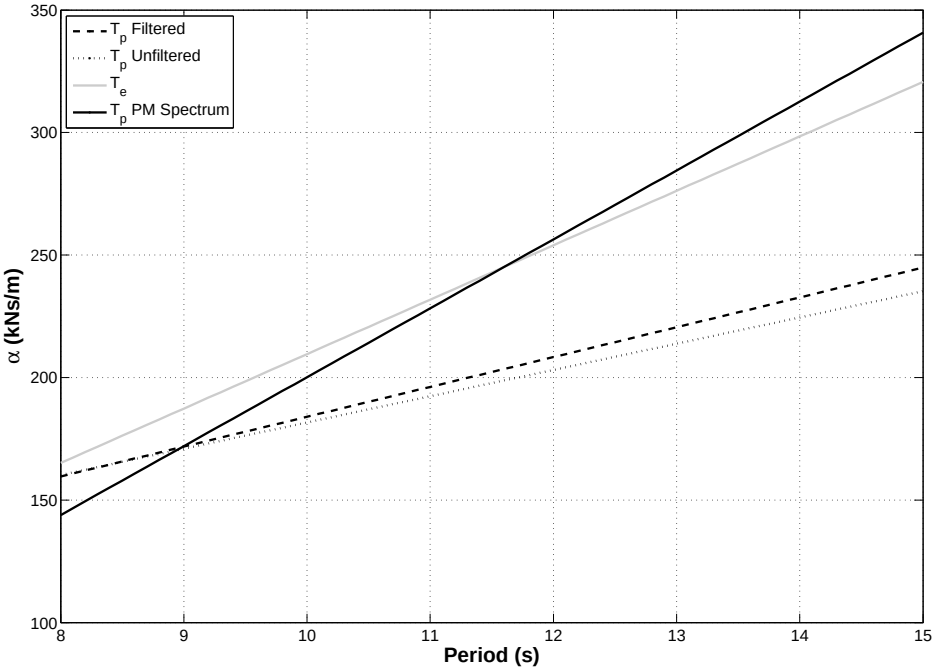

Figure 13: Comparison of the optimum PTO damping trends for the hydraulic PTO for different wave parameters

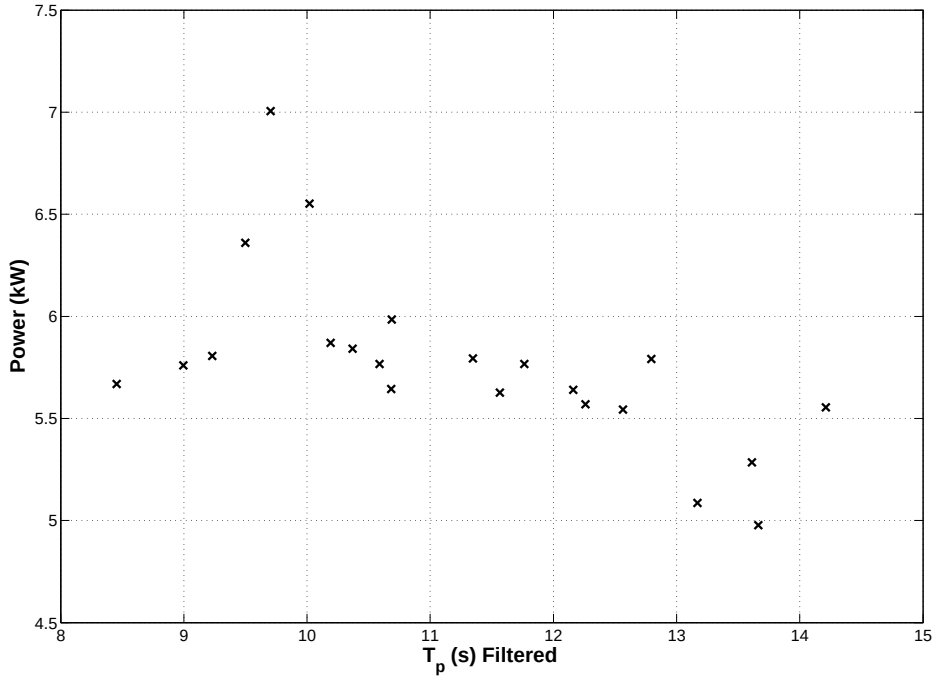

Figure 14: Maximum power generated (P_{gen}) vs peak wave period for the hydraulic PTO

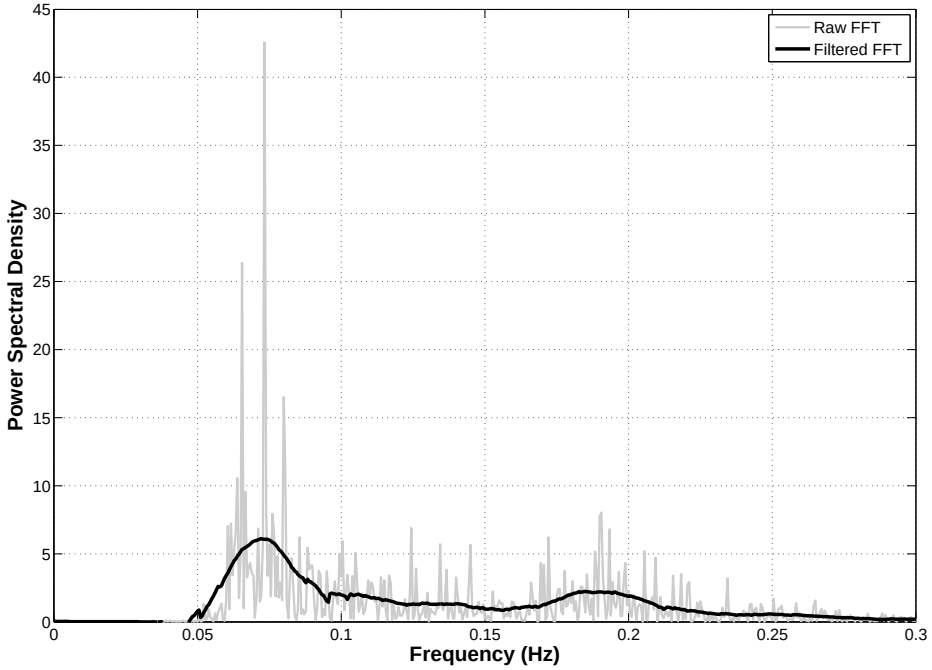

Figure 15: Frequency spectrum of one EMEC file with two distinct peaks

indicates that P_{gen} displays a minor drop with T_p, as previously demonstrated in [3].

Even with filtering, two distinct peaks may remain in the spectrum, like Figure 15, so the PTO may best be tuned to a frequency between these two peaks, instead of the peak frequency, so it can benefit from the high energy at both these frequencies. These types of spectrum are mainly responsible for the outliers in Figures 10 and 11 and are the reason for the poorer correlation. The energy period is less affected by these types of spectrum and therefore produces a better correlation. It should be noted that sea states may exist in which little energy is concentrated at T_p [19], in which case an iterative learning scheme aiming to maximise measured power output by varying PTO and generator parameters would likely perform better.

8. Real Time PTO tuning

Results suggest that a PTO can be tuned to maximise power generation by using T_e over a 30 minute time period. It is therefore beneficial to investigate the most suitable time period to use for tuning the PTO. Four EMEC files, that were not

used previously to determine the tuning trends, are chosen to investigate real time PTO tuning. Their parameters are presented in Table 4 and their filtered spectra are shown in Figure 16.

Wave Parameter	Sea States			
	1	2	3	4
Date & Time	10/04 03:30	21/04 20:30	05/04 13:30	12/04 13:30
H_s (m)	1.24	1.98	3.10	4.34
(Filtered) T_p (s)	11.92	10.34	11.61	12.95
T_e (s)	10.18	9.72	8.83	10.45

Table 4: Parameters of the four EMEC files chosen for the real time PTO tuning

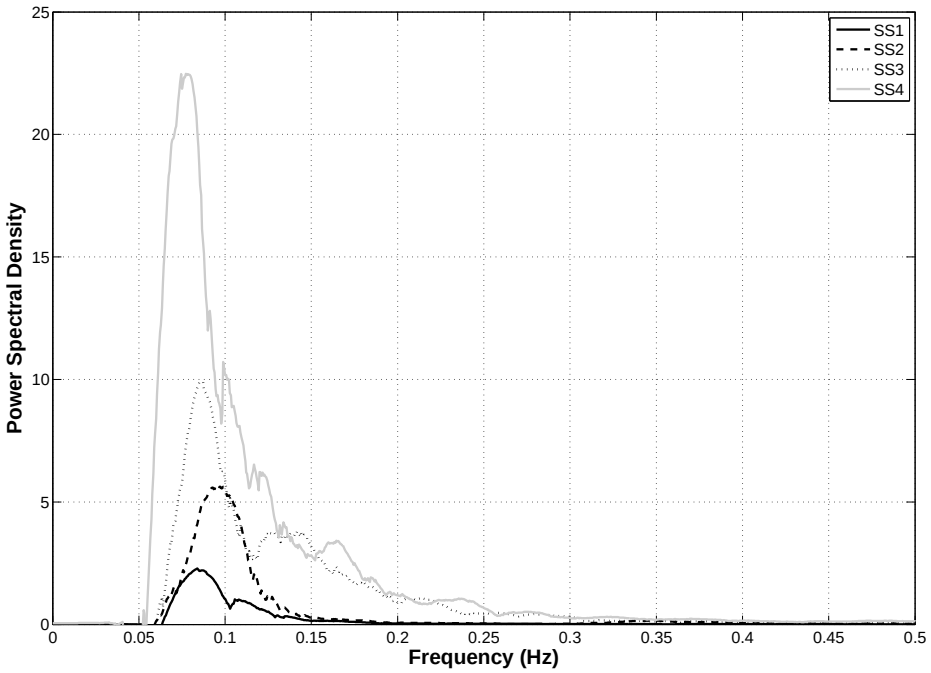

Figure 16: Filtered spectra of the four EMEC files chosen for the real time PTO tuning

Previous work into real time PTO tuning has shown an approximate doubling in power capture with a linear PTO by using an estimated wave frequency, calculated on a 20 s moving average, rather than the constant energy frequency of the spectrum [7]. The estimated wave frequency is calculated using a windowed FFT of the wave displacement. Furthermore, it has been shown that active tuning methods generally outperform passive methods with a linear PTO. Passive methods assume the PTO settings to be fixed whereas the active methods

assume that PTO settings can be constantly varying. In [8], an active tuning technique is used with a 200 s window sliding FFT of the wave displacement. Most recently, work has been presented which illustrates the advantages of estimating the suitable wave frequency information by using signal processing and filtering of the wave displacement signal [20]. It estimates the wave frequency information without future knowledge of the wave profile using the zero-upcrossing method to update the linear PTO settings every 2 - 3 s. The zero-upcrossing method measures each point at which the wave profile crosses the zero line upward. That point is taken as the start of an individual wave and the next zero-upcrossing point is taken as the end of that wave. The time period between the two adjacent zero-upcrossing points is defined as the wave period for that individual wave and the vertical distance between the highest and lowest points between the adjacent zero-upcrossing points is defined as the wave height. In all these examples it is assumed that the PTO is linear and the desired settings are achieved instantly. This work investigates methods to calculate wave frequency information which is then used as the input to an open loop controller for the tuning of the hydraulic PTO. Due to the good linear relationship, the PTO damping (α) is adjusted according to wave energy period T_e (see Figure 12). A base-line passive method uses the PTO damping for the mean site energy frequency (T_e= 9.20 s). The mean site energy frequency is calculated from the two months of data which have been collected. Four active methods are investigated which assume that future prediction of wave displacement at the WEC is not possible, so the PTO is tuned to the energy frequency calculated from a time period (window length) of preceding wave displacement data which is updated every 20 s.

Strategy	Notation	Window Length
Passive	P	Site Average
Active	A1	30 mins
	A2	10 mins
	A3	3 mins
	A4	30 s

Table 5: Parameters of the five tuning strategies for the hydraulic PTO

The use of a doubly-fed induction generator (DFIG) is assumed (as is commonly

used in wind turbines) because they offer variable speed generation in an efficient manner by using a frequency converter [21]. DFIGs have an operational range of approximately ±30% around the synchronous speed of 1500rpm, so it is assumed that if the hydraulic motor speed is outside of this range no power can be transmitted (P_{trans}) to the grid and the generated power is wasted. A generator efficiency of 100% is assumed. To maximise transmitted power, it is necessary to maintain the hydraulic motor speed within the generator speed limits at all times irrespective of wave conditions. The motor speed is controlled by adjusting its displacement (x_m) using a proportional-integral (PI) controller acting on the error in motor speed ω_m from the synchronous value ω_m with $0.1 < x_m < 1.0$. Empirically tuned proportional and integral gains of 0.05 and 0.01 were used. Changes to motor displacement (x_m) will be subject to the dynamics of the swash plate positioning system of the hydraulic piston motor. It is assumed that these dynamics can be modelled as a first order transfer function ($R(s)$) with a time constant, $\tau = 0.1\,\mathrm{s}$, such that

$$R(s) = \frac{1}{1 + 0.1s} \tag{26}$$

To ensure P_{cap} remains at its maximum, $\alpha_{opt}(T_e)$ must be maintained whilst controlling the motor speed. To maintain α_{opt} it is necessary to continually adjust the piston area or generator load at the same rate as x_m. Adjusting the generator load is the only feasible option so it must be varied alongside x_m to maintain α_{opt} according to [3]

$$C_g = \alpha_{opt}(T_e) \left(\frac{x_m D_m}{A_p} \right)^2 \tag{27}$$

Therefore, in the simulation model the signal to alter the generator load is passed through the same transfer function ($R(s)$ or, in practice, an estimate of the real transfer function) to ensure both signals are in phase. The block diagram of this control strategy is shown in Figure 17.

In general, the results show that there is only a marginal gain, if any, from using active tuning methods (Tables 6 to 10). The captured power (P_{cap}) is very similar for all the methods but there are slight variances in the generated (P_{gen})

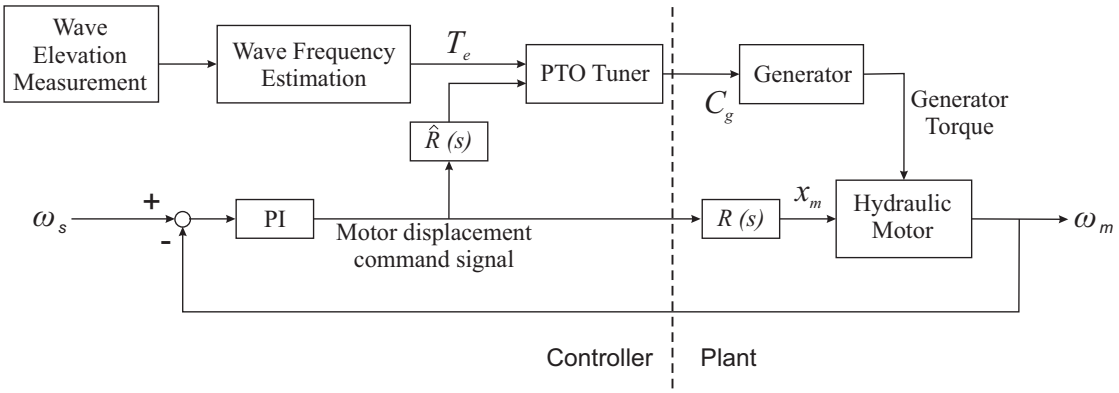

Figure 17: PTO Tuning and Motor Control Block Diagram

Strategy	Power (kW)			Efficiency (%)		
	P_{cap}	P_{gen}	P_{trans}	η_{pto}	η_{trans}	η_{tot}
P	1.13	0.18	0.18	16.2	98.7	16.0
A1	1.11	0.17	0.17	15.6	98.4	15.4
A2	1.12	0.18	0.17	15.7	98.6	15.5
A3	1.10	0.16	0.16	14.6	98.6	14.4
A4	1.10	0.16	0.16	14.6	98.5	14.4

Table 6: Results for SS1 comparing the different tuning methods

Strategy	Power (kW)			Efficiency (%)		
	P_{cap}	P_{gen}	P_{trans}	η_{pto}	η_{trans}	η_{tot}
P	6.21	3.41	3.40	54.8	99.7	54.7
A1	6.17	3.42	3.42	55.4	100	55.4
A2	6.16	3.42	3.42	55.4	100	55.4
A3	6.15	3.41	3.41	55.5	100	55.5
A4	6.16	3.41	3.38	55.3	99.2	55.3

Table 7: Results for SS2 comparing the different tuning methods

Strategy	Power (kW)			Efficiency (%)		
	P_{cap}	P_{gen}	P_{trans}	η_{pto}	η_{trans}	η_{tot}
P	15.7	9.38	6.75	59.6	72.0	42.9
A1	15.8	9.26	6.48	58.6	70.0	41.0
A2	15.8	9.26	6.43	58.6	69.4	40.7
A3	15.8	9.32	6.67	59.0	71.5	42.2
A4	15.7	9.27	6.64	58.9	71.6	42.2

Table 8: Results for SS3 comparing the different tuning methods

Strategy	Power (kW)			Efficiency (%)		
	P_{cap}	P_{gen}	P_{trans}	η_{pto}	η_{trans}	η_{tot}
P	28.2	16.5	4.81	58.5	29.1	17.0
A1	28.3	17.4	6.43	61.4	37.0	22.7
A2	28.3	17.4	6.51	61.6	37.5	23.1
A3	28.3	17.3	6.27	61.2	36.2	22.2
A4	28.2	17.1	5.89	60.5	34.5	20.8

Table 9: Results for SS4 comparing the different tuning methods

Strategy	Sea States				Average
	1	2	3	4	
P	0.18	3.40	6.75	4.82	3.79
A1	0.17	3.42	6.48	6.43	4.12
A2	0.17	3.42	6.43	6.51	4.13
A3	0.16	3.41	6.67	6.27	4.13
A4	0.16	3.38	6.64	5.89	4.02

Table 10: The transmitted power in kW for each sea state using the active and passive tuning methods

and transmitted power (P_{trans}). The biggest gain is for the highest energy sea state (SS4) where the active methods out perform the passive method by at least 20% (in terms of P_{trans}). This is because T_e for SS4 has the biggest difference from the site average value.

Figure 18 shows how the estimated energy period (T_e) and PTO damping (α) vary with time for the different control strategies. For A4 there are large fluctuations in T_e between consecutive discrete values but these variations reduce as the window length of the strategies increases. For SS4 the largest P_{trans} is for method A2. For shorter window lengths, like A4, there can be large transient waves which have a major affect on the estimated T_e. A2 gives a good balance between tracking changes in T_e whilst not being biased by large individual waves. The advantage of using a shorter window length is the reduction in the capacity required to store preceding data but with the passive method there is no requirement for data storage or online calculations. The results for these sea states show only a minor reduction in transmitted power with the passive method, but this would be exacerbated if the energy period differs significantly from the average site value.

By way of illustration, Figure 19 shows a comparison of motor displacement

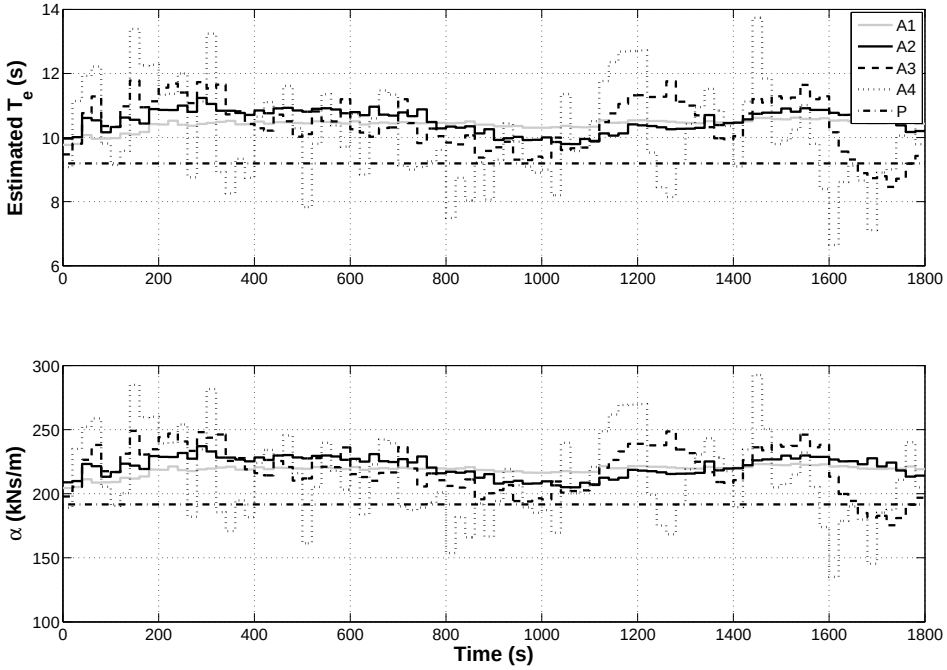

Figure 18: Estimated T_e and corresponding α for the control strategies for SS4

fraction and motor speed for control strategies P and A4 for SS3. This shows how the motor displacement is varied in order to attempt to maintain the synchronous speed of the generator. Figure 20 shows the corresponding transmitted power for the different control strategies. It is clearly seen that transmitted power drops to zero when the synchronous speed limit of ±30% is violated.

9. PTO Tuning To Future Wave Data

Results show that active tuning of the PTO using preceding wave displacement data does not provide a meaningful gain in P_{trans} compared to passive tuning to a mean sea state. If the incident wave displacement could be predicted then power increases could potentially be achieved. Previous work has shown this to be true for a linear PTO [8]. Here we investigate if this is also true for a realistic hydraulic PTO model.

The tuning method predicts T_e from a future window length of 20 s and it uses the previosly identified trend to modify α accordingly. The results, presented in Table 11, indicate that there is only a small gain from using a future wave prediction method when compared to the passive tuning method. The future

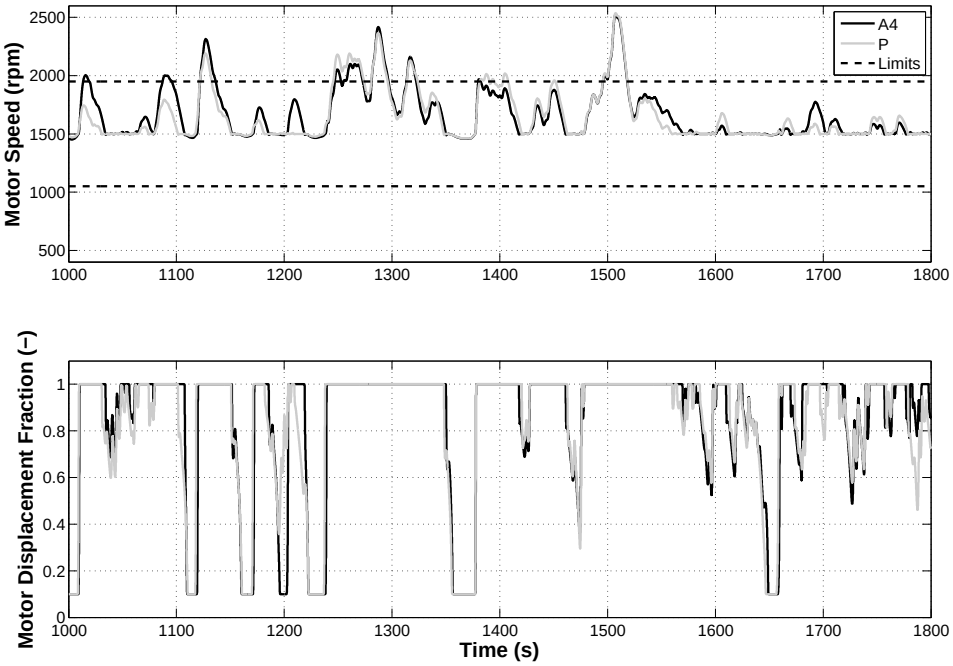

Figure 19: Comparison of motor displacement fraction and motor speed for control strategies P and A4 for SS3

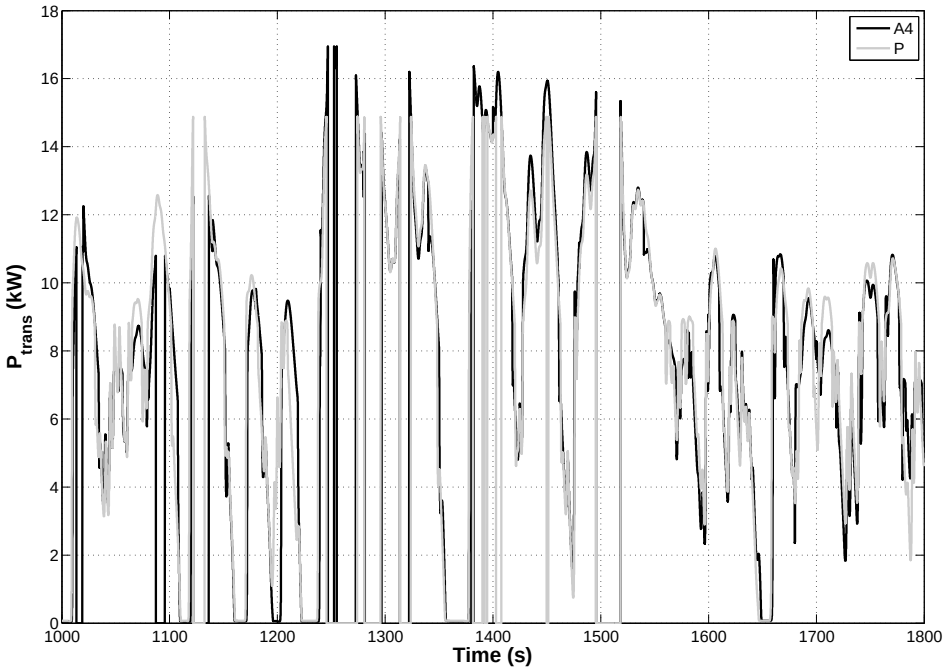

Figure 20: Comparison of transmitted power for control strategies P and A4 for SS3

prediction method only gives a higher transmitted power for SS4 compared to the passive method, but broadly speaking there is minimal change.

Strategy	Power (kW)	Sea States			
		1	2	3	4
Future	P_{cap}	0.97	6.19	15.7	28.4
	P_{gen}	0.11	3.38	8.99	17.1
	P_{trans}	0.10	3.37	5.79	5.41
Passive	P_{cap}	1.13	6.21	15.7	28.2
	P_{gen}	0.18	3.41	9.38	16.53
	P_{trans}	0.18	3.40	6.75	4.82

Table 11: The power for each sea state for the future and passive tuning methods

Therefore, this indicates that there is no gain from using algorithms or nearby measurement buoys to predict the future wave behaviour. Overall, the best tuning method is an active method which determines only a fundamental change in the energy frequency of the waves and therefore gradually changes the PTO damping to tune the device correctly. It is important to note that the presented P_{trans} values are still subject to the inefficiencies of the generator.

10. Conclusions

Wave data for two months in 2011, recorded at the European Marine Energy Centre, was used to derive input data to evaluate tuning strategies for a realistic model of a hydraulic power take-off for a wave energy converter. The model was then used to determine the relationship between the peak wave and energy period and the optimum PTO damping for a number of sea states with varying parameters. An open loop active tuning method was investigated, in which past wave displacement data was used to adjust the PTO damping according to the wave energy frequency. Different window lengths were analysed for the active methods and compared to a passive method in which the PTO is fixed and tuned to the site average frequency. The investigation shows that the tuning of a hydraulic PTO to an estimated wave frequency is a difficult task. Even if the wave frequency can be estimated accurately and the PTO damping adjusted immediately, the PTO force will not change instantly due to the dynamics of the hydraulic PTO. The most effective active method analyses a sufficiently long preceding period of data to determine any change in significant wave frequency but not react to an individual wave. Power generation is expected to improve using active tuning as the energy frequency of the waves deviates further from the average site value. Preview knowledge of the future waves was shown to provide no meaningful improvement in energy capture for a point absorber WEC with a realistic PTO, though it would likely be of value for a wave-by-wave strategy such as latching control.

Finally, the results have illustrated that there is a large power loss in the PTO. This is due to significant power loss in the components of the PTO (especially the hydraulic motor). For example, in low energy seas the small motor displacement required to maintain the synchronous speed means that the motor efficiency is always very low, so the mechanical power that is captured by the PTO can not be converted efficiently. Also, in high energy seas, there is a significant drop between the generated power and the transmitted power because the motor displacement is not large enough to maintain the synchronous speed. Therefore, even though the PTO efficiency may be adequate, a significant

portion of the generated power is lost. Significantly, power gains observed in similar work using simplified linear PTO models and/or simplified sea states are not seen here, demonstrating that over-simplification of the PTO during the simulation phase of WEC development could lead to incorrect design decisions and subsequent additional delay and cost.

References

[1] A.R. Plummer and M. Schlotter. Investigating the Performance of a Hydraulic Power Take-Off. In *Proceedings of the 8th European Wave and Tidal Energy Conference (EWTEC)*, Uppsala, Sweden, 2009.

[2] CJ Cargo, AR Plummer, AJ Hillis, and M Schlotter. Determination of optimal parameters for a hydraulic power take-off unit of a wave energy converter in regular waves. *Proceedings of the Institution of Mechanical Engineers, Part A: Journal of Power and Energy*, 226(1):98–111, 2012.

[3] CJ Cargo, AJ Hillis, and AR Plummer. Optimisation and control of a hydraulic power take-off unit for a wave energy converter in irregular waves. *Proceedings of the Institution of Mechanical Engineers, Part A: Journal of Power and Energy*, 228(4):462–479, 2014.

[4] A.F.O. Falcão. Modelling and control of oscillating-body wave energy converters with hydraulic power take-off and gas accumulator. *Ocean Engineering*, 34(14-15):2021–2032, 2007.

[5] A.F.O. Falcão. Phase control through load control of oscillating-body wave energy converters with hydraulic PTO system. *Ocean Engineering*, 35(3-4):358–366, 2008.

[6] A. Babarit, G. Duclos, and A.H. Clément. Comparison of latching control strategies for a heaving wave energy device in random sea. *Applied Ocean Research*, 26(5):227–238, 2005.

[7] H. Yavuz, A. McCabe, G. Aggidis, and M.B. Widden. Calculation of the performance of resonant wave energy converters in real seas. *Proceedings of*

409 *the Institution of Mechanical Engineers, Part M: Journal of Engineering for*
410 *the Maritime Environment*, 220(3):117–128, 2006.

411 [8] H. Yavuz, T.J. Stallard, A.P. McCabe, and G. Aggidis. Time series
412 analysis-based adaptive tuning techniques for a heaving wave energy
413 converter in irregular seas. *Proceedings of the Institution of Mechanical*
414 *Engineers, Part A: Journal of Power and Energy*, 221(1):77–90, 2007.

415 [9] M. Folley and T. Whittaker. The control of wave energy converters using
416 active bipolar damping. *Proceedings of the Institution of Mechanical*
417 *Engineers, Part M: Journal of Engineering for the Maritime Environment*,
418 223(4):479–487, 2009.

419 [10] A. Babarit, M. Guglielmi, and A.H. Clément. Declutching control of a wave
420 energy converter. *Ocean Engineering*, 36(12):1015–1024, 2009.

421 [11] J. Falnes. *Ocean Waves and Oscillating Systems: Linear Interactions*
422 *including Wave-Energy Extraction*. Cambridge University Press, Cambridge,
423 UK, 2002.

424 [12] A. Hulme. The Wave forces acting on a floating hemisphere undergoing
425 forced periodic oscillations. *The Journal of Fluid Mechanics*, 121:443–463,
426 1982.

427 [13] S. Barstow, G. Mørk, D. Mollison, and J. Cruz. The Wave Energy Resource.
428 In J. Cruz, editor, *Ocean Wave Energy: Current Status and Future*
429 *Perspectives*, chapter 4, pages 93–132. Springer, 2008.

430 [14] W.E. Wilson. Performance criteria for positive displacement pumps and
431 fluid motors. *Trans. Am. Soc. Mech. Eng*, 71(2):115–120, 1949.

432 [15] Edward Pitt. Assessment of Wave Energy Resource. Technical report,
433 European Marine Energy Centre, 2009.

434 [16] A. Savitzky and M.J.E. Golay. Smoothing and Differentiation of Data by
435 Simplified Least Squares Procedures. *Analytical Chemistry*,
436 36(8):1627–1639, 1964.

[17] M.J. Ketabdari and A. Ranginkaman. Simulation of Random Irregular Sea Waves for Numerical and Physical Models Using Digital Filters. *Transaction B: Mechanical Enginerring*, 16(3):240–247, 2009.

[18] AJ Hillis. Active motion control of fixed offshore platforms using an extended state observer. *Proceedings of the Institution of Mechanical Engineers, Part I: Journal of Systems and Control Engineering*, 224(1):53–63, 2010.

[19] A.D. de Andrés, R. Guanche, J. Weber, and R. Costello. Finding gaps on power production assessment on wecs: Wave definition analysis. *Renewable Energy*, 83:171–187, 2015.

[20] H. Yavuz, S. Mistikoglu, and T. Stallard. Processing irregular wave measurements to enhance point absorber power capture performance. *Ocean Engineering*, 38(4):684–698, 2011.

[21] A. Petersson. *Analysis, Modeling and Control of Doubly-Fed Induction Generators for Wind Turbines*. PhD thesis, Chalmers University of Technology, 2005.

Nomenclature

Nomenclature

$A(\omega)$	frequency dependent added mass	[kg]
A_p	piston area	[m^2]
r	buoy radius	[m]
$B(\omega)$	frequency dependent radiation damping coefficient	[Ns/m]
C_f	motor coulomb friction coefficient	[-]
C_g	generator damping coefficient	[Nm/(rad/s)]
C_v	motor viscous friction coefficient	[-]
D_m	motor capacity	[cc/rev]
f_c	coulomb friction	[N]
f_e	wave excitation force	[N]
f_{fr}	cylinder friction	[N]
f_h	wave force	[N]
f_{hs}	wave hydrostatic force	[N]
f_v	viscous friction coefficient	[Ns/m]
f_r	wave radiation force	[N]
$F_e(s)$	Laplace transform of wave excitation force	[N]
g	gravitational acceleration	[ms^{-2}]
H	wave height	[m]
H_s	significant wave height	[m]
J	generator inertia	[kgm^2]
K_v	valve coefficient	[$m^3/s\,bar$]
k	wave number	[m^{-1}]
l	half height of buoy	[m]
m	mass of buoy	[kg]
n	number of wave components	[-]
p_i	piston chamber pressure (i = 1,2)	[bar]
p_A	accumulator 'A' pressure	[bar]
p_B	accumulator 'B' pressure	[bar]
P_{cap}	captured power	[kW]
P_{gen}	generated power	[kW]

P_{trans}	transmitted power	[kW]
P_{wave}	wave power	[kW]
q_m	flow rate to the motor	[m^3/s]
S_n	spectral density	[m^2s]
t	time	[s]
T_m	motor torque	[Nm]
T_p	peak period	[s]
x	buoy displacement	[m]
x_m	fraction of motor displacement	[-]
α	PTO damping	[Ns/m]
α_{opt}	optimum PTO damping	[Ns/m]
Δt	wave cycle time	[s]
$\Delta\omega$	wave frequency band	[rad/s]
ϵ	Havelock's coefficient	[-]
η_{pto}	PTO efficiency	[%]
$\Gamma(\omega)$	wave excitation force coefficient	[N/m]
μ	oil dynamic viscosity	[Ns/m^2]
ρ	water density	[kg/m^3]
Φ	PTO force	[N]
ω	wave frequency	[rad/s]
ω_m	angular motor velocity	[rad/s]
ω_s	generator synchronous velocity	[rad/s]
φ	wave phase component	[s]